

# Spontaneous Charge Oscillations in Dielectric Confined Quasi-2D Systems

Xuanzhao Gao<sup>1,2,\*</sup> and Zecheng Gan<sup>1,3,†</sup>

<sup>1</sup>*Thrust of Advanced Materials, The Hong Kong University of Science and Technology (Guangzhou), Guangdong, China*

<sup>2</sup>*Department of Physics, The Hong Kong University of Science and Technology, Hong Kong SAR, China*

<sup>3</sup>*Department of Mathematics, The Hong Kong University of Science and Technology, Hong Kong SAR, China*

(Dated: March 23, 2023)

We report spontaneous electric field and charge oscillations in dielectric confined Quasi-2D charged systems. A simple relationship is found for the oscillation wave number, which is solely determined by the dielectric mismatch and the length scale of confinement. We analytically show that the emergence of charge/field oscillation is due to the arising of a first-order pole in the quasi-2D Green's function. The oscillatory behavior is further validated numerically, and its influence on collective behaviors of the confined particles is studied via computer simulations. Interestingly, the substrate permittivity alone can trigger spontaneous formations of lattice structures, which may provide new insights in the study of Quasi-2D systems and the design of future nanodevices.

*Introduction.*—Quasi-2D systems are attracting much attention because of their huge potential in future nanodevices. Typically, such systems possess a nano-sized longitudinal thickness in the  $z$  direction, achieved through confinement, bulk-like and modeled as periodic in the transverse  $xy$  directions [1]. Quasi-2D systems exhibit rich new collective behaviors, including polyelectrolyte adsorption and structure [2, 3], ion transport and selectivity [4, 5]. Interestingly, most of these effects are related to the permittivity, also known as the *dielectric confinement effect*. The materials used for nanoscale confinement can range from dielectric to metallic, and nowadays, electromagnetic metamaterials, which have been developed with permittivities that can take negative values [6, 7] when excited by electromagnetic waves of specific frequencies. Great efforts have been made to develop negative permittivity materials in the low frequency limit [8–10]. Noteworthy is that *negative static permittivity* has been achieved recently in a wide range of materials, including metals [11], quasi-2D crystals [12], nano-particles [13], and polymeric systems [14].

The confinement effect turns out to be physically interesting even when only a *single* dielectric substrate is present. Recent calculations have shown that for electrolytes/polymers near a dielectric substrate, the dielectric surface effect can significantly deviate the systems from bulk behaviors, examples include ion transport [15], polymer brush structure [3], and pattern formation in dipolar films [16], where such effect is particularly enhanced when the substrate's permittivity is negative. However, incorporating a second dielectric substrate in the models to actually achieve dielectric confinement in computer simulations is far from straightforward. Although simulation techniques [17–28] have made significant progress in the past few decades, accurate and efficient treatment of the dielectric confinement effect remains challenging.

In this letter, we report evidence for electrostatic field and charge oscillations in Quasi-2D charged systems, triggered by dielectric confinement at nanoscales. We find

a simple physical relationship for the oscillation wave number, which is solely determined by the dielectric mismatch and confinement thickness. The relationship is analyzed theoretically, and also validated numerically under various system settings. Finally, via extensive computer simulations of a prototypical charge- and size-symmetric binary mixture of particles described by the primitive model [29], we reveal that the dielectric confinement can lead to the self organization of charged particles into lattice structures, where its wave number can be well-controlled via the dielectric mismatch and thickness of confinement, consistent with our theoretical predictions.

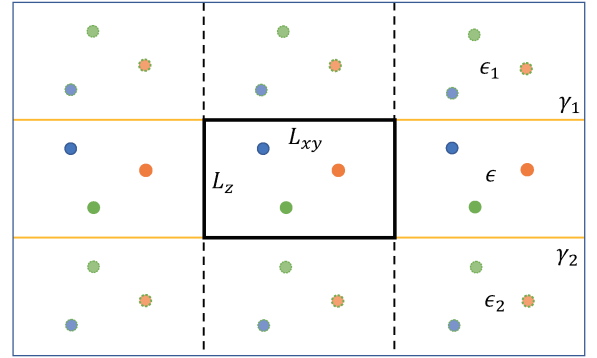


FIG. 1. The figure illustrates a quasi-2D charged system and depicts the dielectric confinement effect from the viewpoint of the Image Charge Method (ICM). The solvent medium, with dielectric permittivity  $\epsilon$ , is represented by the middle layer, while the upper and lower layers represent the substrate with dielectric permittivities of  $\epsilon_1$  and  $\epsilon_2$ , respectively. The real charged particles of the doubly-periodic system are represented by colored circles surrounded by solid lines. The dotted lines represent the image charges that are reflected by the dielectric interfaces in the  $z$  direction.

*The model.*—The modeled geometry of the dielectric confined quasi-2D systems used for simulations is presented in Fig. 1. The system is doubly periodic in the transverse direction and finite in the longitudinal direc-

tion, with edge lengths of  $L_x$ ,  $L_y$ , and  $L_z$ . All charged particles are located between the dielectric substrates with dielectric permittivity  $\epsilon_1$  and  $\epsilon_2$  and are immersed in a solvent with dielectric permittivity  $\epsilon$ . Based on the ICM, the strength of polarization is quantified by the dimensionless coefficient reflection rates,  $\gamma_1$  and  $\gamma_2$ , which are given by  $(\epsilon - \epsilon_i)/(\epsilon + \epsilon_i)$ . The Green's function of Poisson's equation in such systems can be constructed via a multiple reflection process, resulting in an infinite image charge series as schematically illustrated in Fig. 1. Note that when  $|\gamma_1\gamma_2| \leq 1$ , the image reflection series is convergent, but when  $|\gamma_1\gamma_2| > 1$ , it becomes *divergent*, and the reflective ICM approach fails. Therefore, current simulation studies in the  $|\gamma| \geq 1$  regime are limited to a single dielectric substrate [16]. However, our new approach overcomes this divergence issue using a proper renormalization strategy, allowing us to explore the dielectric confinement effect in all possible  $\gamma$  regimes, particularly the less explored scenario of metamaterial substrates with static negative permittivity.

The Green's function  $G(\mathbf{r}, \mathbf{s})$  for Poisson's equation in a dielectric confined quasi-2D system can be expressed as

$$-\nabla \cdot [\eta(\mathbf{r})\nabla G(\mathbf{r}, \mathbf{s})] = 4\pi\delta(\mathbf{r} - \mathbf{s}), \quad (1)$$

where  $\mathbf{r}$  and  $\mathbf{s}$  denote the target and source locations within the confined geometry. It is important to note that the relative dielectric function  $\eta(\mathbf{r}) = \epsilon(\mathbf{r})/\epsilon$  is a piecewise constant, where  $\epsilon(\mathbf{r})$  is the material-specific, spatially varying dielectric constant defined as

$$\epsilon(\mathbf{r}) = \begin{cases} \epsilon_1, & z > L_z \\ \epsilon, & 0 \leq z \leq L_z \\ \epsilon_2, & z < 0 \end{cases}, \quad (2)$$

and depicted in Fig. 1. Furthermore, the dielectric interface conditions require that  $G(\mathbf{r}, \mathbf{s})$  and  $\epsilon(\mathbf{r})\partial_z G(\mathbf{r}, \mathbf{s})$  be continuous across  $z = 0$  and  $L_z$ , with the free-space boundary condition (FBC) holding as  $z \rightarrow \pm\infty$ . It should be noted that proposing the proper FBC for charges under dielectric confinement requires careful consideration to ensure it is physically well-defined, and this will be clarified later. In our discussion, we fix  $\epsilon = 1$  for simplicity, and  $\epsilon_1 = \epsilon_2 = \epsilon'$ , so that  $\gamma_1 = \gamma_2 = \gamma$ . By varying  $\epsilon'$ , we can change  $\gamma$  from  $-10$  to  $10$ . Note that for general dielectric confinement setups with realistic dielectric constants, it is always possible to rescale the dielectric constants by  $\epsilon$  and the confined charge densities by  $\sqrt{\epsilon}$ , so that the electrostatic system is mathematically equivalent. As a possible experimental realization, the permittivity of VO<sub>2</sub> film is approximately  $-14$  at 350K [11]. By choosing solvents with permittivities of approximately 11.4 or 17.1 (such as organic solvents), the proposed  $\gamma$  regimes can be achieved.

*Oscillatory single particle field.*—The dielectric confinement effect turns out to be physically fascinating even in the presence of a single charged particle. In Fig. 2 (a),

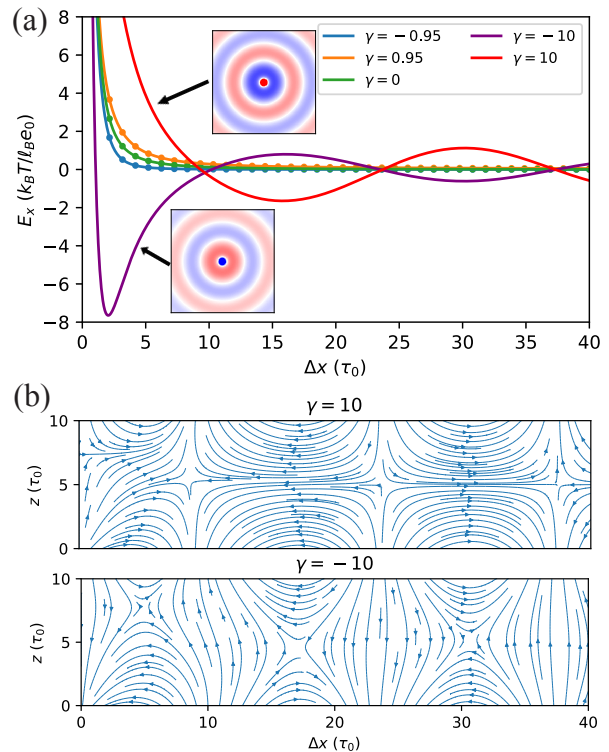


FIG. 2. (a): the electric fields along  $x$  direction, generated by a cation with valence  $\nu = 1$ , fixed at  $z = \tau_0$ , and confined by a pair of dielectric substrates located at  $z = 0$  and  $10\tau_0$ . Subplots depict the polarization charge density on the lower substrates. (b): the corresponding field lines for the  $\gamma = \pm 10$  scenarios.

we present the electric field in the  $x$  direction generated by a cation with valence  $\nu = 1$  located at  $(x_0, y_0, \tau_0)$  in a quasi-2D system with a thickness of  $10\tau_0$ , as a function of the distance from the cation  $\Delta x = x - x_0$ , for different reflection rates  $\gamma$  characterizing the confinement. The field is defined as  $-\nu\ell_B\partial_x G(\mathbf{r}, \mathbf{r}_0)$ , where  $G(\mathbf{r}, \mathbf{r}_0)$  is given by Eq. (10), and  $\ell_B = e_0^2/(4\pi\epsilon_0\epsilon k_B T)$  is the Bjerrum length of the solvent, with  $e_0$  the elementary charge,  $\epsilon_0$  the vacuum permittivity,  $k_B$  the Boltzmann constant, and  $T$  the temperature. For  $|\gamma| < 1$  cases, as illustrated by the blue ( $\gamma = -0.95$ ) and orange ( $\gamma = 0.95$ ) lines in Fig. 2 (a), the polarization weakens or enhances the bare Coulomb field ( $\gamma = 0$ ), but with no qualitative difference. The results obtained by our method are in good agreement with those obtained by ICM, shown in dots in Fig. 2 (a). However, for  $|\gamma| > 1$ , the results become non-trivial and qualitatively different. At short distance, the near field behaves as strongly repulsive or attractive when  $\gamma = 10$  or  $-10$ , respectively, which can be understood as a significant enhancement of the polarization effect for  $|\gamma| < 1$  cases. Even more interesting is the far field, it no longer decays monotonically but exhibits oscillatory behavior, which is rarely reported in previous studies.

To understand the origin of field oscillations, the po-

larization charge density profile on the substrate at  $z = 0$  is shown in the subplots of Fig. 2 (a). The charge density is defined by

$$\sigma(\mathbf{r}) = \lim_{z \rightarrow 0^+} \nu \ell_B \epsilon_0 \left(1 - \frac{\epsilon}{\epsilon'}\right) \partial_z G(\mathbf{r}, \mathbf{r}_0), \quad (3)$$

and the field lines generated by  $\sigma(\mathbf{r})$  are sketched in Fig. 2 (b). The field oscillation is found to be generated by the strong transverse polarization charge density waves, influencing both the near and far fields. The oscillatory field lines has a very similar structure to that of a surface plasmonic resonance wave [30], but the physical origin is different. The oscillation is due to the reflected polarization enhanced by the dielectric confinement, characterized by parameters  $\gamma_1$ ,  $\gamma_2$ , and  $L_z$ . Particularly, The confinement induced oscillation wave number is given by

$$k_0 = \frac{\ln \gamma_1 \gamma_2}{2L_z}, \quad (4)$$

which we will show analytically that this corresponds to a first-order pole in the Sommerfeld integral representation of the Green's function. And the wavelength of the oscillation, defined as two times the distance between nearby zeros, satisfies

$$\lambda \cdot k_0 = 2\pi. \quad (5)$$

Numerical validation shows that Eq. (5) is highly robust under different choices of  $\mathbf{r}$ ,  $\mathbf{r}_0$ ,  $\gamma$ , or  $L_z$ , as shown in Fig. 3. Importantly, the oscillation fields can be accurately predicted and controlled by adjusting  $k_0$ . Eq. (4) also indicates that the oscillation shall be weakened as  $L_z$  is increased, and becomes non-oscillatory when  $\gamma_1 \gamma_2 < 1$ .

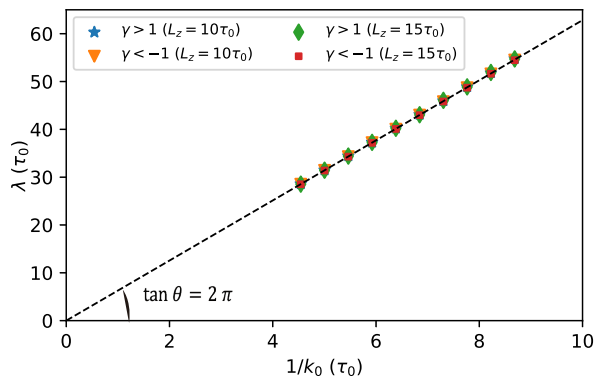


FIG. 3. Numerical validations for the relationship between  $k_0$  and  $\lambda$  under various system parameter settings of  $\gamma$  and  $L_z$ . For each case,  $\lambda$  is approximated by averaging distances between nearby zeros of  $E_x$ , and with different (randomly generated) locations in  $z$ .

*Theoretical origin for oscillations.*—The Green's function problem in Eq. (1) can be solved analytically in

terms of Sommerfeld integrals. Applying plane wave expansion on both sides of Eq. (1) gives,

$$\begin{aligned} G(\mathbf{r}, \mathbf{s}) &= -\frac{1}{\pi} \iint_{\mathbb{R}^2} g(k, z, z_s) e^{-i\mathbf{k} \cdot \Delta \rho} dk_x dk_y \\ &= -\int_0^{+\infty} 2g(k, z, z_s) J_0(k\Delta\rho) k dk, \end{aligned} \quad (6)$$

where  $\mathbf{k} = (k_x, k_y)$ ,  $\Delta \rho = (x - x_s, y - y_s)$ . When  $k > 0$ ,  $g(k, z, z_s)$  is given as

$$g(k, z, z_s) = \frac{1}{2k} \frac{1}{\gamma_1 \gamma_2 \exp(-2kL_z) - 1} \sum_{i=1}^4 \Gamma_i e^{-ka_i}, \quad (7)$$

where  $\Gamma_l = [1, \gamma_1, \gamma_2, \gamma_1 \gamma_2]$  and  $a_l = [|z - z_s|, z + z_s, 2L_z - (z + z_s), 2L_z - |z - z_s|] \in [0, 2L_z]$ . When  $k = 0$ , the solution is given by

$$g(k = 0, z, z_s) = -\frac{|z - z_s|}{2}. \quad (8)$$

Physically, Eq. (8) implies that for  $k = 0$ , confined source charge acts as a uniformly charged plate.

The analytical form of  $g(k, z, z_s)$  indicates that the Sommerfeld integral Eq. (6) has non-trivial behaviors. Clearly,  $g(k, z, z_s)$  is divergent at  $k = k_0$  (given in Eq. (4)), and as  $\gamma_1 \gamma_2$  increases to be larger than 1,  $k_0$  will shift onto the positive real axis, then the Sommerfeld integral needs to be renormalized. Notice that when  $k \rightarrow k_0$ , the divergent factor has the property

$$\frac{1}{\gamma_1 \gamma_2 \exp(-2kL_z) - 1} \rightarrow \frac{1}{2L_z(k_0 - k)}, \quad (9)$$

so that  $k_0$  is a first-order pole and the Cauchy principal value exists. Then Eq. (6) for  $\gamma_1 \gamma_2 > 1$  cases is given by

$$G(\mathbf{r}, \mathbf{s}) = -\text{p.v.} \left[ \int_0^{+\infty} 2g(k, z, z_s) J_0(k\Delta\rho) k dk \right], \quad (10)$$

which can be calculated numerically. In what follows, we analyze the oscillatory behavior (for more details, see Supplementary Information (SI) [31]). First, the Green's function consists of integrals of the following general form

$$I_o = \int_0^{\infty} \frac{J_0(k\Delta\rho) e^{-ka}}{\exp(2L_z(k_0 - k)) - 1} dk, \quad (11)$$

where  $\Delta\rho$ ,  $k_0$  and  $a$  are all positive constants. We find that  $I_o$  can be further expanded as

$$I_o = \frac{e^{-k_0 a}}{2L_z} \int_0^{\infty} \frac{J_0(k')}{k_0 \Delta\rho - k'} dk' + f(k_0, \Delta\rho, a), \quad (12)$$

where  $k' = k\Delta\rho$ , and  $f(k_0, \Delta\rho, a)$  is a non-oscillatory analytic function which has minor contribution to  $I_o$ . The first integral term can be understood as a function of  $k_0 \Delta\rho$ , or denoted as  $I_m(k_0 \Delta\rho)$ . Clearly,  $I_m$  is solely controlled by  $k_0$ , given different parameters of  $\gamma$  and  $L_z$ .

It is found that the first-order pole in  $I_m$  provides the oscillatory mode, and we also numerical validated that the wavelength of the oscillation in  $I_m$  indeed satisfies Eq. (5), which explains our findings.

*Collective behaviors.*—To investigate the influence of field/charge oscillations on the collective behavior of quasi-2D charged systems, we further developed a collection of numerical techniques to efficiently evaluate the Green's function Eq. (6). A novel Ewald-splitting type strategy is proposed, together with renormalization techniques and fast convergent quadrature schemes. All fine details and numerical validations are provided in the SI [31]. Our study focuses on a prototypical quasi-2D charged system, consisting of a binary mixture of charged particles described by the primitive model. The system comprises  $N/2$  cations and  $N/2$  anions, each with the same diameter  $\tau_0$  and valence  $\pm 1$ , resulting in an overall charge-neutral system. The Hamiltonian of the system is defined as follows, where  $i$  represents the  $i$ -th particle with charge  $q_i$  located at position  $\mathbf{r}_i$ :

$$\mathcal{H} = \frac{1}{2} \sum_{i,j=1}^N q_i q_j \ell_B G(\mathbf{r}_i, \mathbf{r}_j) + U_{\text{LJ}}, \quad (13)$$

The sum notation  $\sum_{i,j}$  implies that when  $i = j$ , the function  $G(\mathbf{r}, \mathbf{r})$  corresponds to the self-interaction term, and  $U_{\text{LJ}}$  is the shift-truncated Lennard-Jones (LJ) potential energy used to model excluded-volume interactions. While this model disregards other important interactions observed in experimental realizations, it enables us to isolate the dielectric confinement effect. Similar systems have been studied recently in Refs. [24, 26, 27].

In all the Molecular Dynamics (MD) simulations, we maintain a constant box size in the  $xy$  plane of  $180\tau_0 \times 180\tau_0$ , which is confirmed to eliminate boundary effects. We vary the values of  $L_z$  and  $\gamma$  to adjust the wave number  $k_0$ . The system contains 300 cations and 300 anions. To isolate electrostatic effect, the reduced temperature  $T_r$  is defined as  $T_r = k_B T / \varepsilon_{\text{Coul}}$ , where  $\varepsilon_{\text{Coul}} = e^2 / (4\pi\epsilon(3.5\tau_0))$  and we set  $\varepsilon_{\text{LJ}} = k_B T$  for both particle-particle and particle-substrate interactions. We integrate the temporal evolution using the Velocity-Verlet algorithm provided by LAMMPS [32] and control the temperature using the Anderson thermostat with stochastic collision frequency  $\omega = 0.1$  and reduced temperature  $T_r = 1$ .

Intriguingly, our results demonstrate that the charged particles spontaneously form periodic structures near the substrates for both  $\gamma > 1$  and  $\gamma < -1$  cases, as illustrated in Fig. 4 (a). We attribute the lattice formation to the single particle oscillatory field, which motivates particles self-organizing so as to enhance the overall induced charge landscape into a *checkerboard* structure, with potential wells confining particles nearby to form local clusters. While in the vertical direction, each of the formed clusters on one substrate is paired with another cluster on the opposite side, either anti-symmetrically or symmet-

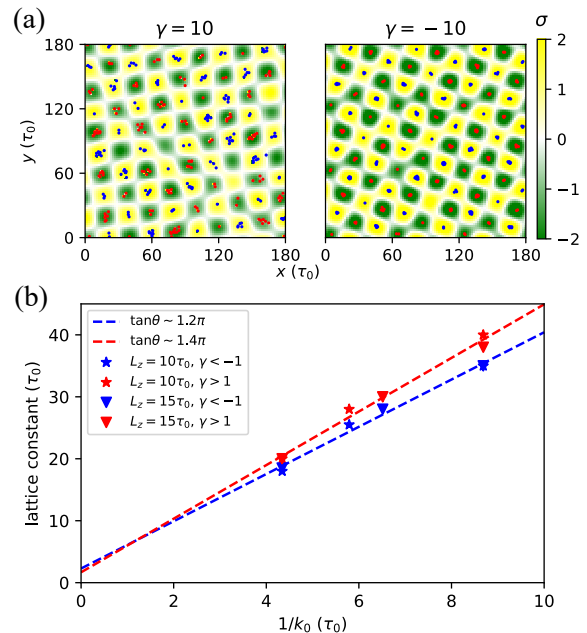


FIG. 4. (a): particle distributions near the lower substrate and induced surface charge densities for  $\gamma = \pm 10$  and  $L_z = 10$ . Positive/negative induced surface charges are in yellow/green, while positive/negative particles are in red/blue, respectively.  $\sigma$  unit:  $e_0/\tau_0^2$ . (b): numerical validations for the relationship between the lattice constant and  $k_0$ . Symbols showing data points from individual simulations, dashed lines depict the linear fitted result.

rically (see Fig. 4 in SI [31]). Two different kind of local cluster structures are observed: for  $\gamma < -1$ , the particles are closely packed into 2D crystal-like structures, while for  $\gamma > 1$ , liquid phase is formed. This can be explained by the strong attractive or repulsive near field generated by a single particle, as was discussed and illustrated in Fig. 2 (a).

Importantly, the formed lattice structure can still be well-controlled via the single parameter  $k_0$ . As shown in Figure 4(b), the lattice constant of the system is found to be proportional to  $k_0^{-1}$ , with various choice of  $L_z$  and  $\gamma$ . Note that two slightly different linear relationships are observed, with fitted slope  $1.2\pi$  and  $1.4\pi$  for  $\gamma < -1$  and  $\gamma > 1$  cases, respectively. The distance between neighboring clusters is found to be consistent with the second zero point of the induced surface charge density profile due to a single point charge (see subplots of Fig. 2 (a)). The mechanism allows one to efficiently modulate the collective phase of dielectric confined systems.

*Conclusions.*—To summarize, we report that dielectric confinement at nanoscales, particularly with negative permittivity values, can induce transverse oscillatory charges and fields. A simple relation for the charge/field oscillation wave number is discovered, which provides new physical insights and has potential in future nan-

odevice design. Efficient algorithms are then developed for efficient simulations of dielectric confined quasi-2D charged systems, by which we show that the oscillatory interaction can further lead to spontaneous lattice structure formations, consistent with theoretical predictions. Future plans include exploration of the phase and transport behavior of dielectric confined systems, fast algorithm for efficient simulations [28, 33], extension to curved/rough substrates, and an open-source implementation in LAMMPS [32].

Z. Gan acknowledges financial support from the National Science Foundation under Award No. CBET-1804940 and DMR-1420073. Z. Gan also wish to thank Aleksandar Donev and Leslie Greengard for helpful discussions on the physics and algorithms for quasi-2D charged systems. X. Gao wish to thank Hongchao Li and Mingzhe Li for fruitful discussions. Both authors want to acknowledge the referees for helpful suggestions in improving this manuscript.

---

\* xz.gao@connect.ust.hk

† Corresponding author; zechenggan@ust.hk

- [1] M. Mazars, Long ranged interactions in computer simulations and for quasi-2D systems, *Phys. Rep.* **500**, 43 (2011).
- [2] R. Messina, Effect of image forces on polyelectrolyte adsorption at a charged surface, *Phys. Rev. E* **70**, 051802 (2004).
- [3] J. Yuan, H. S. Antila, and E. Luijten, Structure of polyelectrolyte brushes on polarizable substrates, *Macromolecules* **53**, 2983 (2020).
- [4] M. Nishizawa, V. P. Menon, and C. R. Martin, Metal Nanotubule Membranes with Electrochemically Switchable Ion-Transport Selectivity, *Science* **268**, 700 (1995).
- [5] J. Cervera, B. Schiedt, R. Neumann, *et al.*, Ionic conduction, rectification, and selectivity in single conical nanopores, *J. Chem. Phys.* **124**, 104706 (2006).
- [6] V. G. Veselago, Electrodynamics of substances with simultaneously negative  $\epsilon$  and  $\nu$ , *Usp Fiziol Nauk* **92**, 517 (1967).
- [7] D. R. Smith, J. B. Pendry, and M. C. Wiltshire, Metamaterials and Negative Refractive Index, *Science* **305**, 788 (2004).
- [8] C. Cheng, R. Fan, Z. Wang, Q. Shao, X. Guo, P. Xie, Y. Yin, Y. Zhang, L. An, Y. Lei, *et al.*, Tunable and weakly negative permittivity in carbon/silicon nitride composites with different carbonizing temperatures, *Carbon* **125**, 103 (2017).
- [9] P. Xie, Z. Shi, M. Feng, K. Sun, Y. Liu, K. Yan, C. Liu, T. A. Moussa, M. Huang, S. Meng, *et al.*, Recent advances in radio-frequency negative dielectric metamaterials by designing heterogeneous composites, *Advanced Composites and Hybrid Materials* **5**, 679 (2022).
- [10] X. Xu, Q. Fu, H. Gu, Y. Guo, H. Zhou, J. Zhang, D. Pan, S. Wu, M. Dong, and Z. Guo, Polyaniline crystalline nanostructures dependent negative permittivity metamaterials, *Polymer* **188**, 122129 (2020).
- [11] J. K. Kana, G. Vignaud, A. Gibaud, and M. Maaza, Thermally driven sign switch of static dielectric constant of VO<sub>2</sub> thin film, *Opt. Mater.* **54**, 165 (2016).
- [12] V. U. Nazarov, Negative static permittivity and violation of Kramers-Kronig relations in quasi-two-dimensional crystals, *Phys. Rev. B* **92**, 161402 (2015).
- [13] J. Shulman, S. Tsui, F. Chen, Y. Xue, and C. Chu, Plasmonic negative capacitance in nanocolloids, *Appl. Phys. Lett.* **90**, 032902 (2007).
- [14] H. Yan, C. Zhao, K. Wang, L. Deng, M. Ma, and G. Xu, Negative dielectric constant manifested by static electricity, *Appl. Phys. Lett.* **102**, 062904 (2013).
- [15] H. S. Antila and E. Luijten, Dielectric Modulation of Ion Transport near Interfaces, *Phys. Rev. Lett.* **120**, 135501 (2018).
- [16] Z. Wang and E. Luijten, Dielectric Modulation of Two-Dimensional Dipolar Materials, *Phys. Rev. Lett.* **123**, 096101 (2019).
- [17] A. Arnold, J. de Joannis, and C. Holm, Electrostatics in periodic slab geometries. I, *J. Chem. Phys.* **117**, 2496 (2002).
- [18] J. de Joannis, A. Arnold, and C. Holm, Electrostatics in periodic slab geometries. II, *J. Chem. Phys.* **117**, 2503 (2002).
- [19] S. Tyagi, A. Arnold, and C. Holm, ICMMM2D: An accurate method to include planar dielectric interfaces via image charge summation, *J. Chem. Phys.* **127**, 154723 (2007).
- [20] A. Fernández-Domínguez, S. Maier, and J. Pendry, Collection and Concentration of Light by Touching Spheres: A Transformation Optics Approach, *Phys. Rev. Lett.* **105**, 266807 (2010).
- [21] V. Jadhao, F. J. Solis, and M. O. De La Cruz, Simulation of Charged Systems in Heterogeneous Dielectric Media via a True Energy Functional, *Phys. Rev. Lett.* **109**, 223905 (2012).
- [22] J. W. Zwanikken and M. Olvera de La Cruz, Tunable soft structure in charged fluids confined by dielectric interfaces, *Proc. Natl. Acad. Sci. U.S.A.* **110**, 5301 (2013).
- [23] F. Fahrenberger and C. Holm, Computing the Coulomb interaction in inhomogeneous dielectric media via a local electrostatics lattice algorithm, *Phys. Rev. E* **90**, 063304 (2014).
- [24] A. P. Dos Santos, M. Giroto, and Y. Levin, Simulations of Coulomb systems confined by polarizable surfaces using periodic Green functions, *J. Chem. Phys.* **147**, 184105 (2017).
- [25] S. Yu and H. Ammari, Plasmonic Interaction between Nanospheres, *SIAM Rev.* **60**, 356 (2018).
- [26] J. Liang, J. Yuan, E. Luijten, and Z. Xu, Harmonic surface mapping algorithm for molecular dynamics simulations of particle systems with planar dielectric interfaces, *J. Chem. Phys.* **152**, 134109 (2020).
- [27] J. Yuan, H. S. Antila, and E. Luijten, Particle-Particle Particle-Mesh algorithm for electrolytes between charged dielectric interfaces, *J. Chem. Phys.* **154**, 094115 (2021).
- [28] O. Maxian, R. P. Peláez, L. Greengard, and A. Donev, A fast spectral method for electrostatics in doubly periodic slit channels, *J. Chem. Phys.* **154**, 204107 (2021).
- [29] W. G. McMillan Jr and J. E. Mayer, The Statistical Thermodynamics of Multicomponent Systems, *J. Chem. Phys.* **13**, 276 (1945).
- [30] K. A. Willets and R. P. Van Duyne, Localized surface plasmon resonance spectroscopy and sensing, *Annu. Rev. Phys. Chem.* **58**, 267 (2007).

- [31] See Supplementary Information at [url] for detailed mathematical derivations, numerical quadrature scheme, its error analysis, and numerical validations, which includes refs. [24, 26, 27, 34]. videos for the MD trajectories are also documented, .
- [32] A. P. Thompson, H. M. Aktulga, R. Berger, *et al.*, LAMMPS - a flexible simulation tool for particle-based materials modeling at the atomic, meso, and continuum scales, *Comp. Phys. Comm.* **271**, 108171 (2022).
- [33] S. Jin, L. Li, Z. Xu, and Y. Zhao, A random batch Ewald method for particle systems with Coulomb interactions, *SIAM J. Sci. Comput.* **43**, B937 (2021).
- [34] L. N. Trefethen, Exactness of Quadrature Formulas, *SIAM Rev.* **64**, 132 (2022).